

SilLang: Improving Gait Recognition with Silhouette Language Encoding

Ruiyi Zhan^{1*}, Guozhen Peng^{1*}, Canyu Chen¹, Jian Lei^{2†}, Annan Li^{1†}

¹Beihang University ²Tsinghua University

{zry, guozhen_peng, chencanyu}@buaa.edu.cn, leij23@mails.tsinghua.edu.cn, liannan@buaa.edu.cn

Abstract

Gait silhouettes, which can be encoded into binary gait codes, are widely adopted to representing motion patterns of pedestrian. Recent approaches commonly leverage visual backbones to encode gait silhouettes, achieving successful performance. However, they primarily focus on continuous visual features, overlooking the discrete nature of binary silhouettes that inherently share a discrete encoding space with natural language. Large Language Models (LLMs) have demonstrated exceptional capability in extracting discriminative features from discrete sequences and modeling long-range dependencies, highlighting their potential to capture temporal motion patterns by identifying subtle variations. Motivated by these observations, we explore bridging binary gait silhouettes and natural language within a binary encoding space. However, the encoding spaces of text tokens and binary gait silhouettes remain misaligned, primarily due to differences in token frequency and density. To address this issue, we propose the Contour-Velocity Tokenizer, which encodes binary gait silhouettes while reshaping their distribution to better align with the text token space. We then establish a dual-branch framework termed Silhouette Language Model, which enhances visual silhouettes by integrating discrete linguistic embeddings derived from LLMs. Implemented on mainstream gait backbones, SilLang consistently improves state-of-the-art methods across SUSTech1K, GREW, and Gait3D.

1. Introduction

Gait recognition is a biometric technique that identifies individuals based on walking patterns. As a non-contact modality, gait can be captured remotely without subject cooperation, which makes it particularly suitable for surveillance and security applications [1, 25, 31].

Since pedestrian gait patterns can be typically represented as binary silhouette sequences obtained through segmentation, which remove non-gait factors such as cloth-

*Equal Contribution.

†Corresponding Author.

Encoding Binary Silhouettes with Silhouette Vocabulary, translating to Silhouette Language.

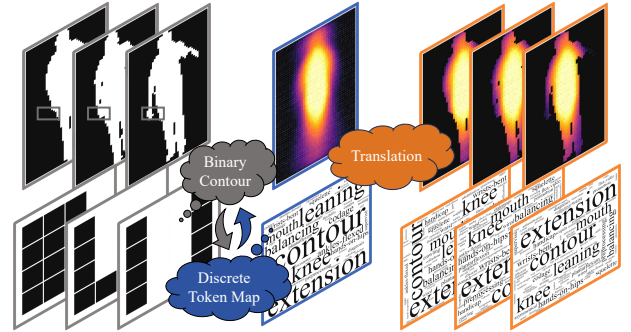


Figure 1. Binary gait silhouettes are encoded with the proposed Contour-Velocity Tokenizer, thereby forming an implicit silhouette vocabulary within the text token space. Since low-frequency silhouette tokens denote subtle walking patterns, shifts in the token frequency distribution capture fine-grained motion cues.

ing variations and maintain the essential motion information, silhouette-based gait recognition has become one of the most widely adopted approaches. Recently, a number of advanced approaches [9, 26, 38, 43] have treated silhouettes as ordinary visual inputs analogous to natural images, employing vision encoders to extract continuous features. Although these methods achieve impressive performance, the continuous encoding inevitably smooths the binary input, disrupting the inherently sparse and discrete nature of gait silhouettes. This limitation indicates the potential benefit of encoding the discrete distribution of silhouettes as a valuable complement to visual encoders. To this end, we explore silhouette encoding schemes that inherently operate in a discrete space.

Notably, the text encoding space in Large Language Models (LLMs) is also sparse and discrete, revealing a natural connection between binary gait silhouettes and language. In LLMs, each word in the predefined vocabulary is represented by a word identifier (ID), typically expressed as a binary one-hot vector, implying that they share a common discrete encoding space. Motivated by this observation, we construct an implicit vocabulary for gait silhouettes, translating motion patterns into silhouette tokens that

can be embedded within the LLM framework. This design enables LLMs to capture subtle silhouette encoding patterns and fine-grained structural dependencies that are frequently overlooked by visual encoders. Leveraging the discrete priors and contextual reasoning abilities of pretrained LLMs [42, 48] therefore provides a promising direction for enhancing visual features of sparse binary gait silhouettes.

Nevertheless, the token density (i.e., the number of tokens required to represent one word or one silhouette) and frequency distribution in binary gait silhouettes differ substantially from those in natural language vocabularies. For instance, a typical sentence of 20 words can be represented by about 20 text tokens, whereas a gait sequence of 30 silhouettes (64×44) requires over 20,000 tokens due to the high pixel redundancy, as illustrated in Figure 1. Therefore, aligning binary silhouettes with the text token space introduces two major challenges: 1) reducing the token density required to represent silhouettes. 2) reshaping the token frequency distribution to better match that of language.

To address these issues, we propose the *Contour-Velocity Tokenizer* (CVT), a novel module that encodes binary gait silhouettes into the text token space. The tokenizer adjusts the intrinsic distribution of binary silhouettes to approximate the statistical properties of natural language and embeds them into a space compatible with LLMs. As shown in Figure 1, the proposed tokenizer establishes an implicit silhouette vocabulary that not only captures the binary structure but also emphasizes fine-grained motion cues, with their most similar tokens in the word vocabulary visualized. By bridging the gap between visual sparsity and linguistic discreteness, we propose a dual-branch framework termed the *Silhouette Language Model* (SilLang). It first converts binary gait silhouette sequences into discrete tokens through the proposed CVT tokenizer. These silhouette tokens are then embedded by an LLM to produce text embeddings, while a lightweight visual branch simultaneously extracts complementary continuous features from the original silhouettes. Finally, a cross-modal alignment and fusion module integrates the textual and visual features into a unified embedding for gait recognition.

The main contributions are summarized as follows:

- **Silhouettes-to-Language Encoding.** We propose CVT tokenizer that directly translates binary silhouettes into discrete tokens, which are then embedded by LLMs.
- **Similarity Analysis.** We provide a theoretical analysis of the structural alignment between silhouettes and natural language, showing that the silhouette encoding space can be regarded as a subset of the linguistic encoding space.
- **Dual-Branch Framework.** We propose SilLang to enhance visual silhouette features by integrating discrete embeddings derived from LLMs. Extensive experiments validate the effectiveness and demonstrate the flexibility of the silhouette language branch, which can be seam-

lessly integrated with different visual gait backbones.

2. Related Works

2.1. Silhouette-based Gait Recognition

Gait recognition identifies individuals through body shapes and motion patterns. To reduce interference from factors such as clothing or carried objects, most recent approaches employ gait silhouettes [5, 6, 8, 9, 15, 20–22, 26, 34–39, 41, 43, 44, 47] for recognition. Specifically, DyGait [37] employs dynamic part learning to extract adaptive local features, GaitBase [8] proposes an efficient backbone for large-scale deployment, and DeepGaitV2 [9] further enhances robustness and scalability through architectural expansion. Furthermore, GLGait [26] designs a global-local temporal receptive field network, and VPNet [22] develops a trainable part-based prompt pool for dynamic incorporation.

In this work, we propose to encode binary gait silhouettes into text token space, enabling pre-trained Large Language Models (LLMs) to enhance visual gait features.

2.2. Gait Recognition with Large Models

Development of LLMs [2, 10, 32] and Multimodal Large Language Models [4, 16] (MLLMs) has introduced new paradigms for cross-modal downstream tasks. CLIP [29] achieves image-text feature alignment through contrastive learning, while LLaVA [18] extends this capability by integrating vision and text features through cross-modal attention mechanisms. Qwen3 [42] further achieves state-of-the-art results across diverse benchmarks, including reasoning, coding, and multilingual understanding. DeepSeek-OCR [40] proposes a unified architecture that reformulates text understanding as a visual modeling task for structured document images.

Recently, large models are applied to gait recognition methods. Specifically, BigGait [45] and BiggerGait [46] extract gait features by large vision models originally designed for general object detection. GaitLLM [43] feeds LLMs with the features extracted from visual gait backbone. However, these frameworks neglect the intrinsic binary attribute of silhouettes, encoding them solely with general vision encoders for subsequent processing. In contrast, we propose CVT to encode binary gait silhouettes into discrete tokens, and directly enhance them by LLMs.

3. Method

3.1. Translate Silhouette into Words

In gait recognition, the walking pattern is usually represented by the silhouettes sequence of pedestrian, which is actually binary image of body contour. The typical size is 64×44 (e.g., in SUSTech1K [30], GREW [50] and Gait3D [49]). Notably, if a binary silhouette is flattened

into a one-dimensional vector (denoted as s), it manifests as a binary code with a bit length of $S_L = \text{height} \times \text{width}$. Since only the contour pixels are meaningful, the binary code is rather sparse which differs substantially from the dense distribution of gray scales of color image. Meanwhile, language models typically employ tokenizers and vocabularies to encode words, mapping words to unsigned integers. Then, each word can be encoded into a one-hot vector with a length equal to the size of the vocabulary (N). The one-hot vector z^k for k -th word in the vocabulary can be encoded as:

$$\mathbf{z}^k = [z_1^k, z_2^k, \dots, z_N^k]^T, \quad (1)$$

where $k \in \{1, 2, \dots, N\}$. And only when $i = k$ does $z_i^k = 1$; in all other cases $z_i^k = 0$. Accordingly, as shown in Figure 2, it can be hypothesized that *the distribution of silhouettes aligns closely with that of language*.

To verify the aforementioned hypothesis, we decompose the vector of flattened silhouette s into the sum of s^k , which is similar to z^k as follows:

$$\mathbf{s}^k = [s_1^k, s_2^k, \dots, s_{S_L}^k]^T, \quad (2)$$

$$\mathbf{s} = \sum_{s_i=1} \mathbf{s}^i \quad \text{where } i \leq S_L, \quad (3)$$

which indicates that the encoding space of silhouette is similar to that of language. Therefore, s can be represented by an unordered set of words when expanding s^k to z^k with a learnable binary matrix $\mathbf{B}_{N \times S_L}$:

$$\begin{aligned} \mathbf{Enc}(s) &= \sum_{s_i=1} \mathbf{B}_{N \times S_L} \mathbf{s}^i \quad \text{where } i \leq S_L \quad (4) \\ &= \sum_{s_i=1} \mathbf{z}^i \quad \text{where } i \leq N, \quad (5) \end{aligned}$$

where \mathbf{Enc} encodes s into a text token space. Specifically, binary gait silhouettes and natural language can be converted into each other when the vocabulary size N equals the number of pixels S_L .

In the context of silhouette-based gait recognition, S_L typically takes a value of 2816 (64×44). However, for instance, N used in Qwen3-Embedding [48] is 151,642, which is far larger than that of S_L . Then, under the condition $S_L < N$, we have $\text{Rank}(\mathbf{B}_{N \times S_L}) = S_L$, which implies that the silhouette encoding space is contained within the language encoding space; consequently, binary gait silhouettes can be encoded into text token space.

Furthermore, incorporating temporal information allows the binary silhouettes to be represented as f ordered aggregated word vectors:

$$\{\mathbf{s}(t)\} = \left\{ \sum_{s^{(t)}_i=1} \mathbf{z}^i \right\} \quad \text{where } t = 1, 2, \dots, f, \quad (6)$$

where f and $s(t)$ refer to the number of frames and the t -th encoded silhouette $\mathbf{Enc}(s)$ of the sequence, respectively.

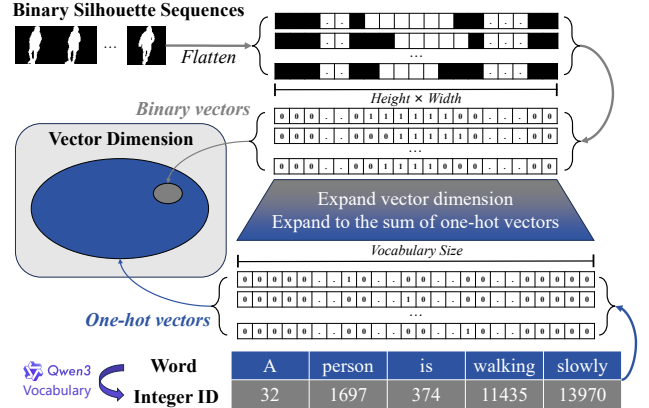


Figure 2. Aligning and translating binary gait silhouettes into natural language within a shared binary encoding space.

Table 1. Analysis of token density in silhouettes, with 1,000 silhouette (64×44) sequences sampled randomly from SUSTech1K [30], GREW [50] and Gait3D [49]. Token density $P_s(1)$, $P_c(1)$, and $P_v(1)$ denote the probabilities of a pixel being 1 in the silhouette, contour map, and velocity map, respectively, approximated by their observed frequencies. ACR represents the Average Compression Rate relative to the original token density.

Density	SUSTech1K	GREW	Gait3D	ACR
$P_s(1)$	21.2%	25.0%	20.2%	100%
$P_c(1)$	4.5%	4.1%	4.1%	19.3%
$P_v(1)$	1.8%	2.0%	2.1%	9.0%

3.2. Contour-Velocity Tokenizer for Silhouette

Token Density and Frequency. While Equation (6) successfully expands s into word vectors, Table 1 shows that the resulting set typically contains more than 500 tokens ($P_s(1) \times S_L$). Such an unusually high number of aggregated words is uncommon in language models, for which we introduce the concept of *token density* (denoted as $P(1)$) to describe tokens in one silhouette. Furthermore, silhouette sequences containing up to 720 frames (the typical maximum used for inference, approximately 360K tokens) substantially increase the token cost, which may exceed the maximum token capacity of the language model (e.g., 32K for Qwen3-Embedding [48]) and is thereby constrained by its ability to process long textual inputs. In addition to token density, we introduce *token frequency* to describe the occurrence frequency of different tokens. As shown in Figure 3 (c), despite differences in token density, the token frequency distributions of text tokens (z^k) and silhouette tokens (s^k) remain distinct. This misalignment in token frequency distribution weakens the ability of language model to capture distinctive motion cues encoded by low-frequency silhouette tokens. To address both issues, we design a *Contour-*

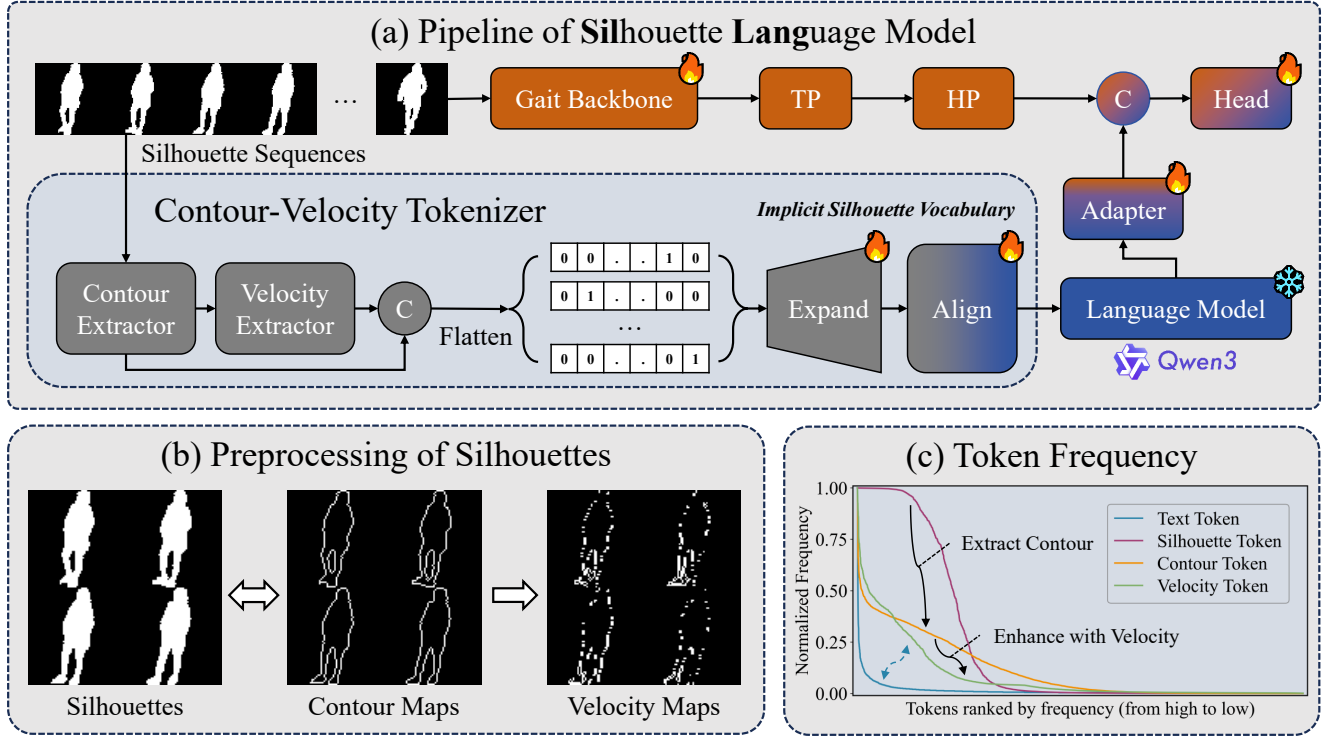


Figure 3. Pipeline of the silhouette language model. (a) The silhouette sequences are encoded with a Contour-Velocity Tokenizer for silhouette language branch, and the Adapter adapts the text embedding (emb_t) to the visual embedding (emb_v). In the visual branch, it keeps the same structure as other silhouette-based gait recognition model [9, 26]. (b) Extract contour map $c(t)$ and velocity map $v(t)$ from silhouette $s(t)$. (c) Visualization of the normalized token frequencies in silhouette and text vocabulary when align silhouette to language.

Velocity Tokenizer for silhouettes, which compresses token density via map extractors and aligns the frequency distribution of silhouette tokens with that of text tokens, thereby constructing an implicit silhouette vocabulary and effectively encoding binary silhouettes into text token space.

Contour Extractor. Since $s(t)$ in Equation (6) reveals that the number of z^i depends on the number of one-hot vectors, where $s(t)_i = 1$. Thus, reducing the token density is equivalent to decreasing the number of TRUE values (white pixels). Considering that the TRUE values within body regions are not that informative in distinguishing subtle walking patterns, we extract the contour map $c(t)$ from $s(t)$ by inverting the interior pixel values to 0 while preserving only the boundary pixels as 1. Results in Table 1 indicate that token density $P_c(1)$ in contour map have been successfully compressed to 19.3% of $P_s(1)$. Furthermore, under the specific data structure of binary pedestrian silhouettes, $c(t)$ and $s(t)$ can be converted into each other losslessly, which is illustrated in Figure 3 (b).

As can be seen, the Contour-Velocity Tokenizer parses $c(t)$ extracted from $s(t)$, without introducing additional information loss. The token frequency distributions of silhouette tokens, contour tokens, and text tokens are compared in Figure 3. It demonstrates that the frequency distribution

of silhouette tokens differs significantly from that of text tokens, whereas the proposed contour extractor effectively shifts it toward that of text tokens.

Velocity Extractor. Although the frequency distribution of contour tokens is closer to that of text tokens, a notable disparity persists, especially within the low-to-mid frequency range. To further address this issue, we extract the differences between frames of $c(t)$ to construct the velocity map $v(t)$. Compared with contour tokens, velocity tokens exhibit a distribution more closely aligned with that of text tokens in the low-to-mid frequency range. This alignment facilitates a clearer distinction between different silhouettes, as it becomes less likely for velocity maps extracted from distinct silhouettes to share the same velocity token. Moreover, as shown in Figure 3 (b) and 3 (c), the velocity map can capture motion as temporal features, thereby enriching the encoded tokens with gait-relevant information. Additionally, as presented in Table 1, velocity tokens exhibit a lower token density (compressed to 9.0%) compared to contour tokens, further narrowing the gap between silhouettes and language.

Expand and Align. After extracting the contour map and velocity map, we encode silhouettes with the contour and velocity tokens, and employ a Multi-Layer Perceptron

Table 2. Recognition results of different embedding fusion methods on Gait3D with DeepGaitV2-P3D.

Fusion method	Rank-1	Rank-5	mAP
Attention	<u>73.3</u>	85.7	<u>64.3</u>
Token Concat	71.4	<u>86.0</u>	63.8
Channel Concat	75.2	87.2	67.1

(MLP) to expand and align the encoded silhouettes with the text token space. Since the token frequency within the contour and velocity maps still shows a slight misalignment with that of text tokens, we introduce a learnable coefficient in the align process to weight each token, thereby balancing the token frequency distribution. The coefficient is initialized as the reciprocal of the frequency of each token and is normalized using the contour frequency, which provides a balanced scaling between static body shape (silhouette tokens) and dynamic motion cues (velocity tokens). The coefficients are estimated from the training set as prior knowledge. Finally, the process is described in Equation (7).

$$token_{sil}(t) = EA(Concat(c(t), v(t))), \quad (7)$$

where EA expands the contour and velocity tokens into the text token space and aligns their frequency distribution with that of text tokens. The resulting $\{token_{sil}(t)|t = 1, 2, \dots, f\}$ are then used as inputs to the language model.

3.3. Exploration on Silhouette Language Model

Since the silhouette sequences in gait datasets (e.g., 18K in Gait3D [49]) are much less than that used for LLM training, while Qwen3-Embedding-0.6B [48] is trained on approximately 150 million pairs of synthetic data. And the silhouettes are of low quality [14, 27, 39], which lead to ambiguous $c(t)$ and $v(t)$, amplifies the noise introduced during the silhouettes extraction process. We propose to frozen the pre-trained LLMs instead of training or finetuning them. Therefore, as illustrated in Figure 3 (a), we adopted a dual-branch architecture for gait recognition. The visual branch follows the design paradigm of mainstream gait recognition models (e.g., DeepGaitV2 [9], GLGait [26]) and consists of four main components [8]: Gait Backbone, Temporal Pooling (TP), Horizontal Pooling (HP), and the recognition Head (Head) [19]. The other one is the silhouette language branch, which enhances the visual feature emb_v obtained from HP module. As shown in Equation (8), emb_{eval} for recognition head fusions emb_t and emb_v from language model and gait backbone, respectively.

$$emb_{eval} = Concat(emb_v, Adapter(emb_t)), \quad (8)$$

where $Adapter$ is an MLP that adapts emb_t to gait recognition task. Furthermore, since the model is not jointly

trained on a sufficiently large and diverse labeled datasets of $s(t)$ - $token_{sil}(t)$ - $text$ pairs, the embedding spaces of emb_v and emb_t are not fully aligned. Consequently, as shown in Table 2, concatenation along the channel dimension yields better performance than attention-based fusion.

4. Experiment

4.1. Datasets and Implementation Details

Gait3D [49] comprises 4,000 subjects, 25,309 sequences, and 3,279,239 frames. Specifically, 3,000 subjects are partitioned for training, while the remaining 1,000 subjects constitute the test set. During the evaluation phase, one sequence from each subject is utilized as the probe, and all remaining sequences form the gallery set.

GREW [50] represents one of the largest gait recognition datasets collected in unconstrained real-world environments. The dataset was acquired using 882 cameras distributed across extensive public areas, amounting to approximately 3,500 hours of $1,920 \times 1,080$ high-resolution streams. In total, it contains 26,345 subjects and 128,671 sequences, which are partitioned into training and test sets comprising 20,000 and 6,000 subjects, respectively.

SUSTech1K [30] is a laboratory-controlled gait dataset acquired using LiDAR sensors and RGB cameras. It comprises 25,239 sequences from 1,050 subjects and covers a wide range of variations, including visibility, views, occlusions, clothing, carrying, and scenes.

Implementation Details. In our experiments, we employ Qwen3-Embedding-0.6B [48] as the language model for the silhouette language branch. For the visual branch, we adopt DeepGaitV2-P3D [9] and GLGait [26] as the backbones. For Gait3D and GREW, DeepGaitV2-P3D is configured with a 22-layer architecture, while GLGait uses the large model (GLGait-L [26]). Since SUSTech1K contains only 250 identities in the training set, a 10-layer configuration of DeepGaitV2-P3D is adopted to avoid overfitting.

In the training stage, the input silhouettes are resized to 64×44 , which is simultaneously fed into two parallel branches. The optimizer is Stochastic Gradient Descent (SGD), while the weight decay and the momentum are set to 0.0005 and 0.9. And the parameters of language model are frozen, while other parameters remain trainable. CTL [26] from GLGait is used for Gait3D and GREW, while triplet [13] and cross-entropy [23] loss are used for SUSTech1K. Then, we train the model with a batch size of 32×4 (4 sequences for each pedestrian, 32 pedestrians in total) on Gait3D and GREW, while 8×8 on SUSTech1K. 1) On Gait3D, the training iteration is 120k. The learning rate starts at 0.1 and is subsequently decreased by a factor of 0.1 at iterations (40k, 80k, 100k). 2) On GREW, the training iteration is 180k. The learning rate starts at 0.05 and is subsequently decreased by a factor of 0.2 at iterations (60k,

Table 3. Comparison of Rank-1, 5 accuracy and mean Average Precision (%) on Gait3D and GREW, where *-P3D and *-GL refer to the gait backbone, DeepGaitV2-P3D and GLGait, respectively. The superscript † denotes results obtained using 128 channels, whereas our experiments are conducted with 64 channels due to limited computational resources.

Method	Publication	Gait3D			GREW	
		Rank-1	Rank-5	mAP	Rank-1	Rank-5
GaitSet [3]	AAAI 2019	36.7	58.3	30.0	46.3	63.6
GaitPart [7]	CVPR 2020	28.2	47.6	21.6	44.0	60.7
GaitGL [17]	ICCV 2021	29.7	48.5	22.3	47.3	63.6
SMPLGait [49]	CVPR 2022	53.2	71.0	42.4	-	-
DyGait [37]	ICCV 2023	66.3	80.8	56.4	71.4	83.2
HSTL [36]	ICCV 2023	61.3	76.3	55.5	62.7	76.6
GaitGCI [6]	CVPR 2023	57.2	74.5	45.0	68.5	80.8
GaitBase [8]	CVPR 2023	64.6	79.6	55.5	60.1	74.5
QAGait [39]	AAAI 2024	67.0	81.5	56.5	59.1	-
CLTD [41]	ECCV 2024	69.7	85.2	-	78.0	87.8
GaitMoE [15]	ECCV 2024	73.7	-	66.2	79.6	89.1
VPNet [22]	CVPR 2024	75.4	87.1	-	80.0	89.4
GLGait [26]	MM 2024	<u>77.6</u> (77.7 [†])	88.4 (88.9 [†])	<u>69.6</u> (70.6 [†])	80.0 (82.8 [†])	89.4 (91.1 [†])
WaveLoss [38]	AAAI 2025	75.6	88.4	66.5	-	-
DeepGaitV2-P3D [9]	TPAMI 2025	74.4 (75.0 [†])	88.0	65.8	77.7	87.9
GaitLLM-P3D [43]	CVPR 2025	76.5	88.1	68.3	79.8	89.5
SilLang-P3D	Ours	76.9	<u>88.2</u>	68.8	<u>80.6</u>	<u>89.9</u>
SilLang-GL		78.4	87.8	70.3	81.2	90.1

Table 4. Results with different attributes on SUSTech1K, where * indicates that the method is reproduced with the same configuration.

Method	Probe Sequence (Rank-1)								Overall Rank-1
	Normal	Bag	Clothing	Carrying	Umbrella	Uniform	Occlusion	Night	
GaitSet [3]	69.1	68.3	37.4	65.0	63.1	61.0	67.2	23.0	65.0
GaitPart [7]	62.2	62.8	33.1	59.5	57.3	54.9	57.2	21.8	59.2
GaitGL [17]	67.1	66.2	35.9	63.3	61.6	58.1	66.6	17.9	63.1
GaitBase [8]	81.5	77.5	49.6	75.8	75.6	76.7	81.4	25.9	76.1
DeepGaitV2-P3D* [9]	86.9	82.4	48.9	79.2	83.3	81.8	85.0	27.7	80.1
GaitLLM-P3D* [43]	<u>86.4</u>	<u>83.1</u>	<u>53.1</u>	<u>80.5</u>	<u>85.3</u>	<u>83.9</u>	<u>88.0</u>	<u>27.7</u>	<u>81.6</u>
SilLang-P3D (Ours)	86.3	83.2	53.6	81.1	85.7	85.0	88.1	28.3	82.0

120k, 150k). 3) On SUSTech1K, the training iteration is 50k. The learning rate starts at 0.1 and is subsequently decreased by a factor of 0.1 at iterations (20k, 30k, 40k).

4.2. Performance Comparison

We integrate SilLang with silhouette-based gait backbones, including DeepGaitV2-P3D [9] and GLGait [26], which are denoted as SilLang-P3D and SilLang-GL, respectively. This section presents a comparison between SilLang and other state-of-the-art gait recognition methods on the Gait3D, GREW, and SUSTech1K datasets, evaluated by Rank-1, 5 accuracy and mean Average Precision (mAP).

Improvement on Metrics. As shown in Table 3, Sil-

Lang achieves consistent improvements across multiple gait silhouette datasets. Specifically, our best results reach 78.4% and 81.2% in Rank-1 accuracy on the Gait3D and GREW datasets, respectively. When integrated with the DeepGaitV2-P3D, SilLang-P3D improves Rank-1 accuracy and mAP on Gait3D by +2.5% and +3.0%, and increases Rank-1 accuracy on GREW by +2.9%.

Furthermore, as shown in Table 4, when applied to the SUSTech1K dataset, SilLang-P3D further enhances model robustness to diverse variations, and increases the overall Rank-1 accuracy by +1.9%. These results demonstrate that the language-encoded silhouettes effectively enhances the discriminative capability of the model across diverse and

Table 5. Ablation study on components of the Contour-Velocity Tokenizer, including the velocity extractor ($v(t)$) and dimension expansion and align module (EA).

$v(t)$	EA	Rank-1	Rank-5	mAP
✗	✗	73.7	87.1	64.9
✗	✓	74.0	88.1	<u>66.2</u>
✓	✗	<u>74.5</u>	86.9	<u>66.2</u>
✓	✓	75.2	<u>87.2</u>	67.1

Table 6. Ablation study on branches selected for training, where the Backbone and LLM refer to the gait backbone (DeepGaitV2-P3D) and the large language model (Qwen3-Embedding-0.6B).

Backbone	LLM	Rank-1	Rank-5	mAP
✗	✗	71.6	<u>86.8</u>	64.4
✗	✓	72.1	86.1	64.0
✓	✗	75.2	87.2	67.1
✓	✓	<u>73.5</u>	87.2	<u>65.4</u>

Table 7. Ablation study on silhouette vocabulary size S_L (pixels), where - is the reproduced baseline without language model.

S_L ($Height \times Width$)	Rank-1	Rank-5	mAP
-	74.2	<u>86.9</u>	67.1
704 (32×22)	<u>74.7</u>	86.6	<u>65.6</u>
2816 (64×44)	75.2	87.2	67.1

challenging scenarios.

Effectiveness on Different Backbones. SilLang also exhibits strong generalization capability across various backbone architectures, including both 3D CNN-based [12, 28] DeepGaitV2-P3D and Transformer-based [33] GLGait. As shown in Table 3, the consistent improvements observed across different architectures indicate that the silhouette language branch provides complementary information to the visual branch. Specifically, while the visual gait backbone smooths continuous pixel variations and shows limited sensitivity to fine contour details, the proposed tokenizer amplifies these discrete motion cues, enabling the LLM to embed them more distinctly and complement the visual features.

Moreover, since the silhouette language is derived directly from binary gait silhouettes, SilLang introduces no dependency on external data sources, thereby avoiding the limitations and quality constraints typically associated with additional modalities.

4.3. Ablation Study

All ablation studies are conducted on the Gait3D dataset using SilLang-P3D. The experiments reported in Table 5,

Table 8. Ablation study on different LLM size.

Language Model	Rank-1	Rank-5	mAP
Qwen-Embedding-0.6B	<u>76.9</u>	<u>88.2</u>	<u>68.8</u>
Qwen-Embedding-4B	77.2	88.8	69.3

Table 6, and Table 7 are trained for 60K iterations to reduce computational overhead and training time. In contrast, the results in Table 8 are obtained after 120K iterations to further demonstrate the embedding capability of larger LLMs.

Effect of the Contour-Velocity Tokenizer. The effectiveness of proposed tokenizer is shown in Table 5. As illustrated in Figure 3 (b), since $s(t)$ and $c(t)$ are equivalent representations, we focus on $v(t)$ and the EA module.

The results indicate that both components contribute positively to recognition accuracy. The velocity map $v(t)$ enriches fine-grained motion representations by incorporating temporal cues, whereas the EA module further aligns the token frequency distribution. This expand and align process essentially constructs an implicit silhouette vocabulary that maps contour and velocity tokens into the text token space, thereby enabling more effective exploitation of the contextual embedding capability of LLMs.

Training Branch Configuration. Table 6 compares different configurations for freezing and training the visual gait backbone and the LLM. The best performance is achieved when the LLM is frozen and only the gait backbone is trained. This configuration offers two main advantages. First, the silhouette dataset contains only about 18K[49] sequences for the silhouette language branch, which may cause overfitting if the LLM is trained jointly. Second, the silhouette language branch primarily acts as a feature enhancer, leveraging sparse and discrete cues embedded from LLMs, which complement the continuous features extracted by the visual branch. Moreover, Freezing the LLM preserves its pretrained representational capacity, while training the gait backbone facilitates better alignment between visual and text embedding space.

Size of the Silhouette Vocabulary. Results in Table 7 indicate that a larger silhouette vocabulary further improves performance. This improvement can be attributed to the increased embedding capacity afforded by a larger vocabulary, which expands the vector space to capture more combinations of tokens representing motion patterns.

Scaling Behavior of the Silhouette Language Model. As shown in Table 8, the results demonstrate the impact of LLM size on performance, revealing that larger models consistently yield higher performance. Specifically, Qwen3-Embedding with 0.6B and 4B parameters set embedding dimensions to 1024 and 2560, respectively, whereas each gait silhouette contains 2816 pixels. Results indicate that a higher dimension can reduce information loss during the

compression from tokens to the LLM embedding space, thereby enabling richer and more discriminative representations that further improve performance.

4.4. Visualization

To further validate the effectiveness of SiLLang, we visualize the token similarity between silhouettes and natural language, as well as the changes in embedding distance before and after incorporating the silhouette language branch.

Token Similarity of Silhouette and Language. As illustrated in Figure 4, we compare the normalized distributions of the visual embeddings (emb_v), silhouette language embeddings (emb_t), text embeddings, encoded silhouette tokens ($token_{sil}$) and text tokens. emb_v , emb_t and $token_{sil}$ are extracted from silhouettes in the Gait3D [49] dataset, while the text embeddings and tokens are obtained by encoding natural language text through Qwen3-Embedding-0.6B [48].

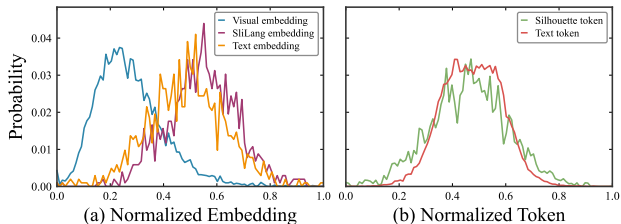


Figure 4. Distribution of normalized embeddings and tokens across different branches. (a) Embeddings in visual, silhouette language and text branches; (b) Input tokens for LLMs.

In Figure 4 (a), emb_t obtained from the language model exhibit a distribution closely aligned with that of text embeddings, while both differ substantially from the visual embeddings emb_v . This observation indicates that SiLLang preserves the embedding capability of the LLM. In Figure 4 (b), the encoded silhouettes tokens $token_{sil}$ show a distribution highly similar to that of text tokens, confirming the similarity between silhouettes and language. This suggests that silhouettes can be encoded as a structure-driven language. Moreover, the results validate that the *EA* module successfully constructs an effective silhouette vocabulary.

Analysis of the Improving Accuracy. As shown in Figure 5, SiLLang substantially improves Rank-1 accuracy for short sequences (1–100 frames). This improvement arises because the training process employs a fixed input length of 30 frames, indicating that the *Adapter* in silhouette language branch effectively adapts the emb_t tailored to a specific sentence length. Moreover, incorporating the SiLLang increases the distance between positive and negative sample embeddings, thereby improving class separability and enhancing recognition accuracy.

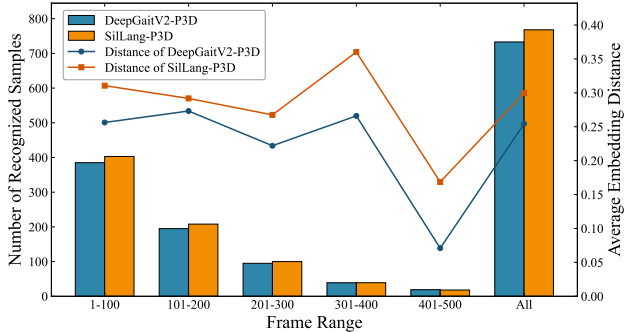


Figure 5. Performance improvement of SiLLang on Gait3D. The number of correctly recognized samples in test set are partitioned according to the frame-length ranges. And the average distance is defined as the mean distance between negative samples minus that between positive samples within each frame-length range.

4.5. Discussion

Our findings suggest that sparse visual data and natural language share fundamental commonalities in encoding complexity and representation discreteness within their encoding spaces. Similar to DeepSeek-OCR [40], which demonstrates that visual models can be extended to text understanding, our work shows that language models can, conversely, embed sparsely encoded binary gait silhouette images. This structural symmetry implies that both modalities may operate within comparable basis vector spaces, enabling the unification of visual sparsity and linguistic discreteness. Furthermore, ESM3 [11] and Evo [24] extract discrete tokens from proteins and DNA based on amino-acid and nucleotide sequences, supporting that discrete data can be encoded within LLM frameworks. Such a perspective not only explains the effectiveness of proposed SiLLang but also points to new opportunities for integrating sparse visual and linguistic representations within a shared encoding framework.

5. Conclusion

Gait silhouettes are represented as binary images and can be encoded into binary gait codes, sharing a discrete and sparse vector space similar to word vocabularies. This structural similarity enables LLMs to enhance continuous visual gait features using sparse text-driven embeddings, while allowing gait recognition models to capture fine-grained temporal motion variations induced by subtle contour and velocity shifts across frames. However, the token density and frequency distributions differ between silhouette and text tokens. To address this, we propose the Contour-Velocity Tokenizer that adjusts these distributions and effectively constructs an implicit silhouette vocabulary. Experimental results demonstrate that binary gait silhouettes can be translated into language, thereby enhancing gait representations and the recognition performance.

References

- [1] Imed Bouchrika, Michaela Goffredo, John Carter, and Mark Nixon. On using gait in forensic biometrics. *Journal of forensic sciences*, 56(4):882–889, 2011. 1
- [2] Tom Brown, Benjamin Mann, Nick Ryder, Melanie Subbiah, Jared D Kaplan, Prafulla Dhariwal, Arvind Neelakantan, Pranav Shyam, Girish Sastry, Amanda Askell, et al. Language models are few-shot learners. *NeurIPS*, 33:1877–1901, 2020. 2
- [3] Hanqing Chao, Kun Wang, Yiwei He, Junping Zhang, and Jianfeng Feng. Gaitset: Cross-view gait recognition through utilizing gait as a deep set. *IEEE TPAMI*, 44(7):3467–3478, 2021. 6
- [4] Gheorghe Comanici, Eric Bieber, Mike Schaekermann, Ice Pasupat, Noveen Sachdeva, Inderjit Dhillon, Marcel Blisstein, Ori Ram, Dan Zhang, Evan Rosen, et al. Gemini 2.5: Pushing the frontier with advanced reasoning, multimodality, long context, and next generation agentic capabilities. *arXiv preprint arXiv:2507.06261*, 2025. 2
- [5] Muqing Deng, Zhuyao Fan, Peng Lin, and Xiaoreng Feng. Human gait recognition based on frontal-view sequences using gait dynamics and deep learning. *IEEE TMM*, 26:117–126, 2024. 2
- [6] Huanzhang Dou, Pengyi Zhang, Wei Su, Yunlong Yu, Yining Lin, and Xi Li. Gaitgci: Generative counterfactual intervention for gait recognition. In *CVPR*, pages 5578–5588, 2023. 2, 6
- [7] Chao Fan, Yunjie Peng, Chunshui Cao, Xu Liu, Saihui Hou, Jiannan Chi, Yongzhen Huang, Qing Li, and Zhiqiang He. Gaitpart: Temporal part-based model for gait recognition. In *CVPR*, pages 14225–14233, 2020. 6
- [8] Chao Fan, Junhao Liang, Chuanfu Shen, Saihui Hou, Yongzhen Huang, and Shiqi Yu. Opengait: Revisiting gait recognition towards better practicality. In *CVPR*, pages 9707–9716, 2023. 2, 5, 6
- [9] Chao Fan, Saihui Hou, Junhao Liang, Chuanfu Shen, Jingzhe Ma, Dongyang Jin, Yongzhen Huang, and Shiqi Yu. Opengait: A comprehensive benchmark study for gait recognition towards better practicality. *IEEE TPAMI*, 2025. 1, 2, 4, 5, 6
- [10] Daya Guo, Dejian Yang, Haowei Zhang, Junxiao Song, Ruoyu Zhang, Runxin Xu, Qihao Zhu, Shirong Ma, Peiyi Wang, Xiao Bi, et al. Deepseek-r1: Incentivizing reasoning capability in llms via reinforcement learning. *arXiv preprint arXiv:2501.12948*, 2025. 2
- [11] Thomas Hayes, Roshan Rao, Halil Akin, Nicholas J Sofroniew, Deniz Oktay, Zeming Lin, Robert Verkuil, Vincent Q Tran, Jonathan Deaton, Marius Wiggert, et al. Simulating 500 million years of evolution with a language model. *Science*, 387(6736):850–858, 2025. 8
- [12] Kaiming He, Xiangyu Zhang, Shaoqing Ren, and Jian Sun. Deep residual learning for image recognition. In *CVPR*, pages 770–778, 2016. 7
- [13] Alexander Hermans, Lucas Beyers, and Bastian Leibe. In defense of the triplet loss for person re-identification, 2017. 5
- [14] Saihui Hou, Xu Liu, Chunshui Cao, and Yongzhen Huang. Gait quality aware network: toward the interpretability of silhouette-based gait recognition. *IEEE Transactions on Neural Networks and Learning Systems*, 34(11):8978–8988, 2022. 5
- [15] Panjian Huang, Yunjie Peng, Saihui Hou, Chunshui Cao, Xu Liu, Zhiqiang He, and Yongzhen Huang. Occluded gait recognition with mixture of experts: an action detection perspective. In *ECCV*, pages 380–397. Springer, 2024. 2, 6
- [16] Aaron Hurst, Adam Lerer, Adam P Goucher, Adam Perelman, Aditya Ramesh, Aidan Clark, AJ Ostrow, Akila Welihinda, Alan Hayes, Alec Radford, et al. Gpt-4o system card. *arXiv preprint arXiv:2410.21276*, 2024. 2
- [17] Beibei Lin, Shunli Zhang, and Xin Yu. Gait recognition via effective global-local feature representation and local temporal aggregation. In *ICCV*, pages 14648–14656, 2021. 6
- [18] Haotian Liu, Chunyuan Li, Qingyang Wu, and Yong Jae Lee. Visual instruction tuning. *NeurIPS*, 36:34892–34916, 2023. 2
- [19] Hao Luo, Youzhi Gu, Xingyu Liao, Shenqi Lai, and Wei Jiang. Bag of tricks and a strong baseline for deep person re-identification. In *Proceedings of the IEEE/CVF conference on computer vision and pattern recognition workshops*, pages 0–0, 2019. 5
- [20] Kang Ma, Ying Fu, Dezhi Zheng, Chunshui Cao, Xuecai Hu, and Yongzhen Huang. Dynamic aggregated network for gait recognition. In *CVPR*, pages 22076–22085, 2023. 2
- [21] Kang Ma, Ying Fu, Dezhi Zheng, Yunjie Peng, Chunshui Cao, and Yongzhen Huang. Fine-grained unsupervised domain adaptation for gait recognition. In *ICCV*, pages 11313–11322, 2023.
- [22] Kang Ma, Ying Fu, Chunshui Cao, Saihui Hou, Yongzhen Huang, and Dezhi Zheng. Learning visual prompt for gait recognition. In *CVPR*, pages 593–603, 2024. 2, 6
- [23] Shie Mannor, Dori Peleg, and Reuven Rubinfeld. The cross entropy method for classification. In *ICML*, pages 561–568, 2005. 5
- [24] Eric Nguyen, Michael Poli, Matthew G Durrant, Brian Kang, Dhruva Katrekar, David B Li, Liam J Bartie, Armin W Thomas, Samuel H King, Garyk Brix, et al. Sequence modeling and design from molecular to genome scale with evo. *Science*, 386(6723):eado9336, 2024. 8
- [25] Mark S Nixon and John N Carter. Automatic recognition by gait. *Proceedings of the IEEE*, 94(11):2013–2024, 2007. 1
- [26] Guozhen Peng, Yunhong Wang, Yuwei Zhao, Shaoxiong Zhang, and Annan Li. Glgait: a global-local temporal receptive field network for gait recognition in the wild. In *ACM MM*, pages 826–835, 2024. 1, 2, 4, 5, 6
- [27] Guozhen Peng, Yunhong Wang, Shaoxiong Zhang, Rui Li, Yuwei Zhao, and Annan Li. Rsnnet: Relative-sequence quality assessment network for gait recognition in the wild. *Pattern Recognition*, 161:111219, 2025. 5
- [28] Zhaofan Qiu, Ting Yao, and Tao Mei. Learning spatio-temporal representation with pseudo-3d residual networks. In *ICCV*, pages 5533–5541, 2017. 7
- [29] Alec Radford, Jong Wook Kim, Chris Hallacy, Aditya Ramesh, Gabriel Goh, Sandhini Agarwal, Girish Sastry, Amanda Askell, Pamela Mishkin, Jack Clark, et al. Learning transferable visual models from natural language supervision. In *ICML*, pages 8748–8763. Pmlr, 2021. 2

- [30] Chuanfu Shen, Chao Fan, Wei Wu, Rui Wang, George Q Huang, and Shiqi Yu. Lidargait: Benchmarking 3d gait recognition with point clouds. In *CVPR*, pages 1054–1063, 2023. [2](#), [3](#), [5](#), [11](#)
- [31] Chuanfu Shen, Shiqi Yu, Jilong Wang, George Q Huang, and Liang Wang. A comprehensive survey on deep gait recognition: Algorithms, datasets, and challenges. *IEEE Transactions on Biometrics, Behavior, and Identity Science*, 2024. [1](#)
- [32] Hugo Touvron, Thibaut Lavril, Gautier Izacard, Xavier Martinet, Marie-Anne Lachaux, Timothée Lacroix, Baptiste Rozière, Naman Goyal, Eric Hambro, Faisal Azhar, et al. Llama: Open and efficient foundation language models. *arXiv preprint arXiv:2302.13971*, 2023. [2](#)
- [33] Ashish Vaswani, Noam Shazeer, Niki Parmar, Jakob Uszkoreit, Llion Jones, Aidan N Gomez, Łukasz Kaiser, and Illia Polosukhin. Attention is all you need. *NeurIPS*, 30, 2017. [7](#)
- [34] Jilong Wang, Saihui Hou, Yan Huang, Chunshui Cao, Xu Liu, Yongzhen Huang, and Liang Wang. Causal intervention for sparse-view gait recognition. In *ACM MM*, pages 77–85, 2023. [2](#)
- [35] Jilong Wang, Saihui Hou, Yan Huang, Chunshui Cao, Xu Liu, Yongzhen Huang, Tianzhu Zhang, and Liang Wang. Free lunch for gait recognition: A novel relation descriptor. In *ECCV*, pages 39–56. Springer, 2024.
- [36] Lei Wang, Bo Liu, Fangfang Liang, and Bincheng Wang. Hierarchical spatio-temporal representation learning for gait recognition. In *ICCV*, pages 19582–19592. IEEE, 2023. [6](#)
- [37] Ming Wang, Xianda Guo, Beibei Lin, Tian Yang, Zheng Zhu, Lincheng Li, Shunli Zhang, and Xin Yu. Dygait: Exploiting dynamic representations for high-performance gait recognition. In *ICCV*, pages 13424–13433, 2023. [2](#), [6](#)
- [38] Zicheng Wang and Qiuxia Wu. Waveloss: An adaptive dynamic loss for deep gait recognition. In *AAAI*, pages 8259–8267, 2025. [1](#), [6](#)
- [39] Zengbin Wang, Saihui Hou, Man Zhang, Xu Liu, Chunshui Cao, Yongzhen Huang, Peipei Li, and Shibiao Xu. Qagait: Revisit gait recognition from a quality perspective. In *AAAI*, pages 5785–5793, 2024. [2](#), [5](#), [6](#)
- [40] Haoran Wei, Yaofeng Sun, and Yukun Li. Deepseek-ocr: Contexts optical compression. *arXiv preprint arXiv:2510.18234*, 2025. [2](#), [8](#)
- [41] Haijun Xiong, Bin Feng, Xinggang Wang, and Wenyu Liu. Causality-inspired discriminative feature learning in triple domains for gait recognition. In *ECCV*, pages 251–270. Springer, 2024. [2](#), [6](#)
- [42] An Yang, Anfeng Li, Baosong Yang, Beichen Zhang, Binyuan Hui, Bo Zheng, Bowen Yu, Chang Gao, Chengen Huang, Chenxu Lv, et al. Qwen3 technical report. *arXiv preprint arXiv:2505.09388*, 2025. [2](#)
- [43] Shaopeng Yang, Jilong Wang, Saihui Hou, Xu Liu, Chunshui Cao, Liang Wang, and Yongzhen Huang. Bridging gait recognition and large language models sequence modeling. In *CVPR*, pages 3460–3469, 2025. [1](#), [2](#), [6](#)
- [44] Lingxiang Yao, Worapan Kusakunniran, Peng Zhang, Qiang Wu, and Jian Zhang. Improving disentangled representation learning for gait recognition using group supervision. *IEEE TMM*, 25:4187–4198, 2023. [2](#)
- [45] Dingqiang Ye, Chao Fan, Jingzhe Ma, Xiaoming Liu, and Shiqi Yu. Biggait: Learning gait representation you want by large vision models. In *CVPR*, pages 200–210, 2024. [2](#)
- [46] Dingqiang Ye, Chao Fan, Zhanbo Huang, Chengwen Luo, Jianqiang Li, Shiqi Yu, and Xiaoming Liu. Biggait: Unlocking gait recognition with layer-wise representations from large vision models. *arXiv preprint arXiv:2505.18132*, 2025. [2](#)
- [47] Weichen Yu, Hongyuan Yu, Yan Huang, and Liang Wang. Generalized inter-class loss for gait recognition. In *ACM MM*, pages 141–150, 2022. [2](#)
- [48] Yanzhao Zhang, Mingxin Li, Dingkun Long, Xin Zhang, Huan Lin, Baosong Yang, Pengjun Xie, An Yang, Dayiheng Liu, Junyang Lin, Fei Huang, and Jingren Zhou. Qwen3 embedding: Advancing text embedding and reranking through foundation models, 2025. [2](#), [3](#), [5](#), [8](#)
- [49] Jinkai Zheng, Xinchun Liu, Wu Liu, Lingxiao He, Chenggang Yan, and Tao Mei. Gait recognition in the wild with dense 3d representations and a benchmark. In *CVPR*, pages 20228–20237, 2022. [2](#), [3](#), [5](#), [6](#), [7](#), [8](#), [11](#), [12](#)
- [50] Zheng Zhu, Xianda Guo, Tian Yang, Junjie Huang, Jiankang Deng, Guan Huang, Dalong Du, Jiwen Lu, and Jie Zhou. Gait recognition in the wild: A benchmark. In *ICCV*, pages 14789–14799, 2021. [2](#), [3](#), [5](#), [11](#)

Supplementary Material for *SilLang: Improving Gait Recognition with Silhouette Language Encoding*

6. Additional Visualizations

6.1. Token Density and Frequency

The frequency heatmaps of silhouette tokens $s(t)$, contour tokens $c(t)$, and velocity tokens $v(t)$ across Gait3D [49], GREW [50], and SUSTech1K [30] are presented in Figure 6. In these heatmaps, the area of the high-intensity regions indicates the token density, whereas the intensity within these regions represents the token frequency. To maintain a consistent brightness range across token types, the heatmaps are normalized according to the frequency range of $c(t)$, as $c(t)$ exhibits an intermediate distribution between the much higher frequencies of $s(t)$ and the substantially lower frequencies of $v(t)$.

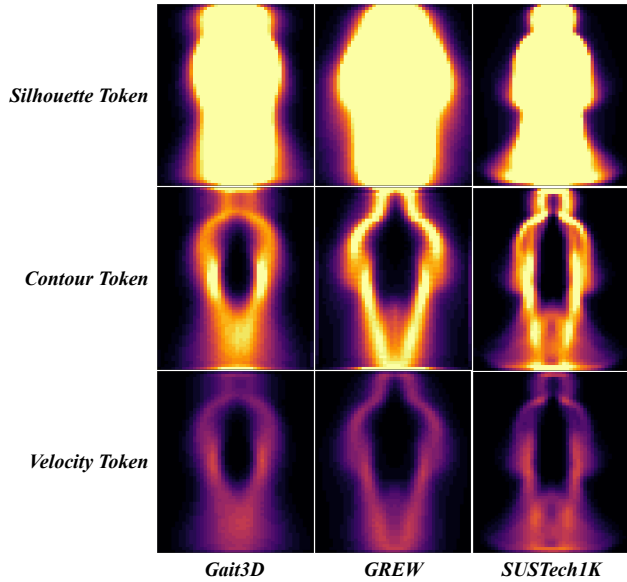


Figure 6. Normalized frequency heatmaps of $s(t)$, $c(t)$, and $v(t)$ on Gait3D [49], GREW [50], and SUSTech1K [30].

In the normalized heatmaps, the three token types exhibit a consistent pattern across all datasets, demonstrating the robustness of the proposed CVT tokenizer. The silhouette token density $P_s(1)$ within each frame is exceedingly high, far surpassing the contour token density $P_c(1)$, which itself remains considerably higher than the velocity token density $P_v(1)$. Spatially, contour tokens concentrate along human-body boundaries, forming a distinct contour band, while velocity tokens exhibit a similar boundary-aligned pattern but with much lower frequency. These observations indicate that the proposed CVT tokenizer reduces the excessive density of silhouette tokens and enhances low-to-mid frequency

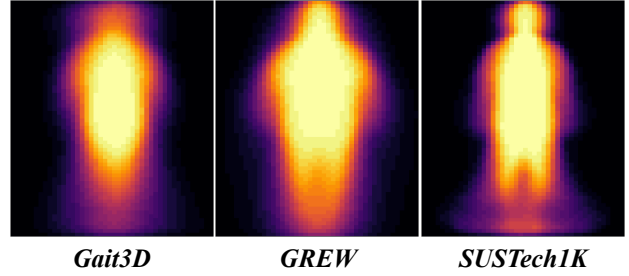


Figure 7. Original frequency heatmaps of $s(t)$ on Gait3D [49], GREW [50] and SUSTech1K [30].

signals, enabling the capture of subtle contour and motion shifts that silhouette tokens alone can hardly encode.

As shown in Figure 7, the original frequency heatmaps exhibit slight variations in token distributions across datasets, indicating that the statistical properties of silhouette, contour, and velocity tokens are dataset dependent. Future work may therefore explore the design of a cross-dataset adaptive tokenizer that first distills dataset-invariant gait characteristics and then adjusts token distributions to match different datasets. Another promising direction is to jointly train the silhouette tokenizer on multiple datasets, which would enhance its generalization ability and mitigate dataset-induced distribution bias. In addition, future research may explore data augmentation strategies that make fuller use of the black (inactive) regions in silhouettes to expand the diversity of token patterns within the silhouette vocabulary. Such strategies would not only reduce the overly high frequencies of silhouette tokens but also activate the low-frequency regions, enabling more complete use of the entire token space. These efforts may facilitate a more balanced frequency distribution and promote a closer alignment with the statistical properties of natural language.

6.2. Silhouette Vocabulary

As shown in Figure 8, the silhouette vocabulary is constructed by measuring the embedding similarity between encoded silhouette tokens and thousands of text tokens. Since the encoded silhouette tokens are not solely used to represent silhouette, their composition implicitly encodes information about the individual and motion pattern, which can be interpreted as a compound word. Moreover, within this token embedding space, multiple encoded silhouette tokens can correspond to the same text token, allowing similar tokens to represent different compound words, which is consistent with the properties of the silhouette vocabulary described above.

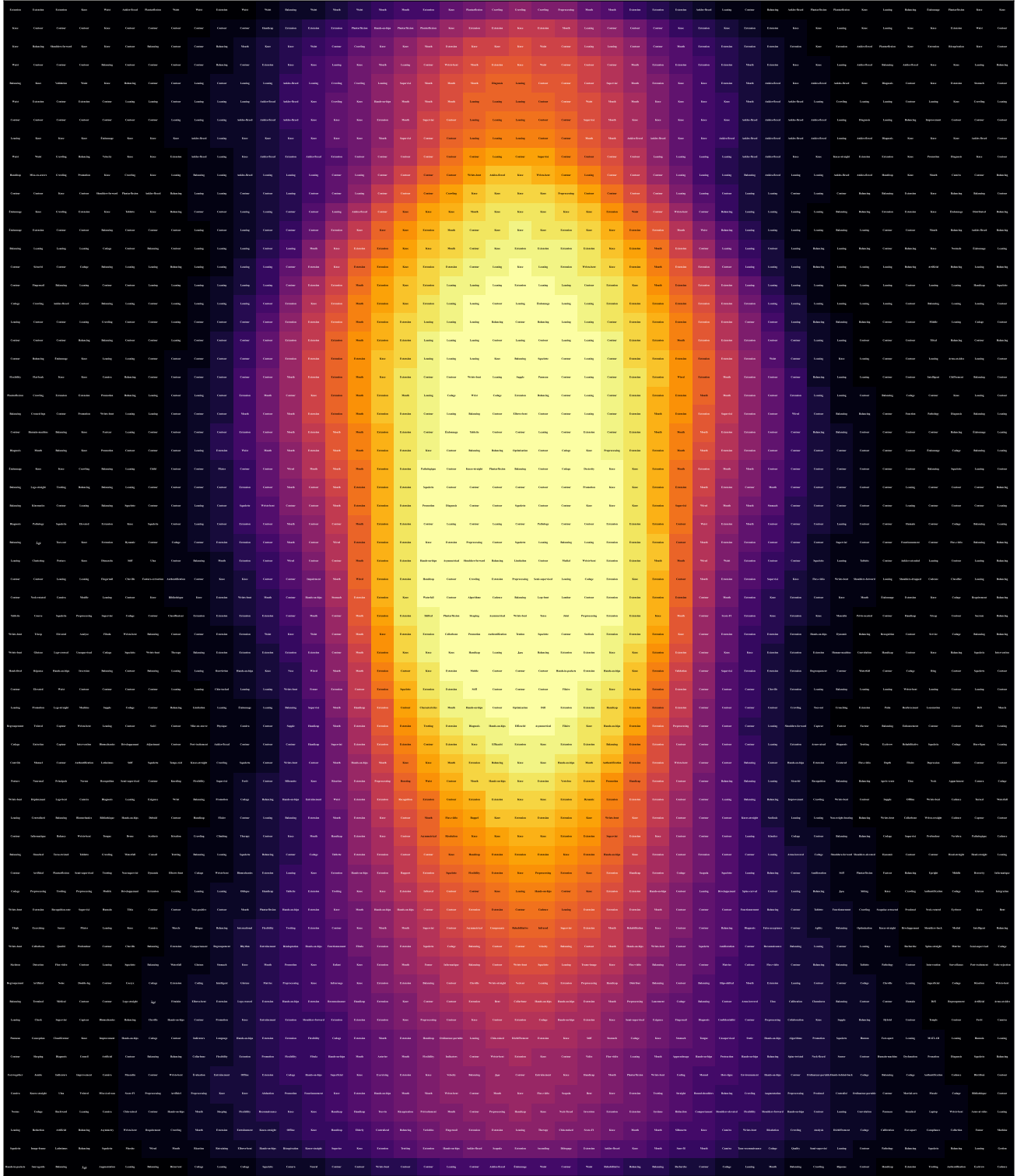


Figure 8. Visualization of the silhouette vocabulary (64×44). The frequency heatmap is extracted from Gait3D [49]. These text tokens are not directly provided as encoded silhouette tokens to the LLMs, which are measured by embedding similarity of tokens for visualization.